INVESTIGATION INTO ELECTRON CLOUD EFFECTS IN THE ILC DAMPING RING DESIGN

J.A. Crittenden, J. Conway, G.F. Dugan, M.A. Palmer and D.L. Rubin
CLASSE,* Cornell University, Ithaca, NY 14850, USA

K. Harkay, L. Boon
ANL, Argonne, IL 60439, USA

M.A. Furman
LBNL, Berkeley, CA 94720, USA

S. Guiducci
LNF, Frascati, Italy

M.T.F. Pivi, L. Wang
SLAC, Menlo Park, CA 94025, USA

Abstract

We report modeling results for electron cloud buildup in the ILC damping ring lattice design. Updated optics, wiggler magnets, and vacuum chamber designs have recently been developed for the 5 GeV, 3.2-km racetrack layout. An analysis of the synchrotron radiation profile around the ring has been performed, including the effects of diffuse and specular photon scattering on the interior surfaces of the vacuum chamber.

DESIGN OF THE DTC03 LATTICE

The racetrack layout for the 3238-m circumference ILC damping ring design has recently been updated, and is now referred to as the DTC03 lattice. The 100-m-long RF straight can accommodate as many as 16 single-cell cavities and the 226-m wiggler straight up to 60 superferric wigglers [1]. The baseline design (26-ms damping time and 5-Hz operation) requires 8 cavities with total accelerating voltage of 14 MV and 54 2.1-m-long wigglers with 1.51-T peak field. To run in the 10-Hz mode, the wigglers operate at 2.16 T in order to cut the radiation damping time in half, and the accelerating voltage is increased to 22.4 MV with 12 cavities to preserve the 6-mm bunch length. The 339-m phase trombone, in the same straight, consists of five six-quadrupole cells and has a tuning range of ± 0.5 betatron wavelengths. The opposite straight includes injection and extraction lines, and the 117-m-long chicane for fine adjustment of the revolution period. The range of the chicane is ± 4.5 mm with negligible contribution to the horizontal emittance. The arc cell is a simple variation of a TME-style cell with a single 3-m bend, three quadrupoles, one focusing and two defocusing, for a total length of 9.7 m. There are 75 cells in each arc.The dynamic aperture including magnet multipole errors and misalignments, and wiggler nonlinearities, is large enough to accept the phase space of the injected positrons, defined so that $A_x + A_y < 0.07$ m-rad (normalized) and $\Delta E/E \leq 0.075\%$ [2].

* Work supported by National Science Foundation and by the US Department of Energy under contract numbers PHY-0734867, PHY-1002467 and DE-FC02-08ER41538,DE-SC0006505

VACUUM CHAMBER DESIGN

A conceptual design of the vacuum chambers for the ILC positron damping ring has been completed in preparation for the ILC Technical Design Report. The design incorporates mitigation techniques in each magnetic field region to suppress the buildup of the electron cloud (EC) in the vacuum chambers of the ring. The mitigation methods were selected based on the results of an intense research effort conducted as part of the ILC Technical Design program [3]. The vacuum system conceptual design is described in Ref. [4]. In the arc regions of the ring, the 50-mm aperture vacuum chambers utilize TiN-coating to suppress the secondary electron yield (SEY) of the chambers, and dual antechambers to reduce the number of photoelectrons entering the central region. The rear walls of the antechambers are angled as well. In the dipoles, the EC is further suppressed by the use of longitudinal grooves on the top and bottom surfaces. In the wiggler region, a 46-mm aperture chamber utilizes clearing electrodes in the wigglers to suppress growth of the cloud and dual antechambers along with custom photon stops to suppress the generation of photoelectrons. In the straights of the dogleg ring, the 50-mm aperture round vacuum chamber is TiN-coated for secondary suppression. Drift regions throughout the ring will employ solenoid windings to further suppress cloud buildup near the beam.

PHOTON TRANSPORT MODEL

The distribution of synchrotron radiation photon absorption sites around the ring can be used to predict the sources of the photoelectrons which seed the EC. This distribution

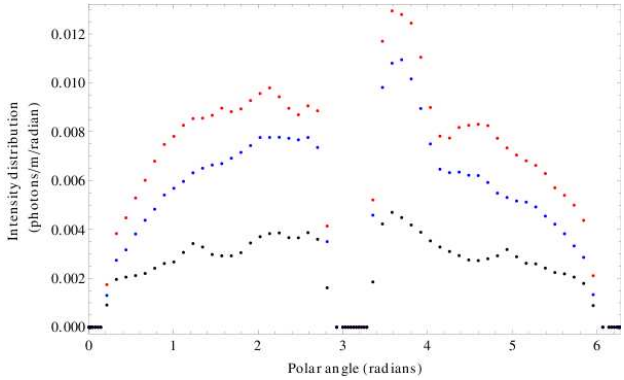

Figure 1: Intensity distributions for absorbed photons in one arc of the damping ring, averaged over three types of magnetic environments. The average over the quadrupole regions is shown in red. The average over the field-free regions is shown in blue and the average over the dipole regions is shown in black. The angle is defined to be zero where the vacuum chamber intersects the bend plane on the outside of the ring. The angle $\pi/2$ corresponds to the top of the vacuum chamber.

has been computed for the DTC03 lattice using a newly developed photon-tracking simulation code, Synrad3D [5]. This code computes the synchrotron radiation photons per electron generated by a beam circulating in the magnetic lattice, and simulates the propagation in three dimensions, of the photons as they scatter off, or are absorbed by, the vacuum chamber. The design vacuum chamber geometry, including details such as antechambers and photon stops, is used in the calculation. Both specular and diffuse photon scattering are included in the simulation. For the scattering calculation, the surface material is approximated as aluminum with a thin carbon coating, and the surface parameters are representative of a typical technical vacuum chamber, namely rms rougness 100 nm and correlation length 5000 nm.

Figure 1 shows the photon intensity distributions for magnetic elements in one of the arcs of the damping ring. The low photon rates at zero and π radians are due to the antechambers. The top-bottom asymmetry is due to a non-vertical slope introduced in the antechamber back walls to inhibit scattering out of the antechamber.

EC BUILDUP IN THE ARC DIPOLES

Using the code POSINST, we have simulated the EC buildup in the arc dipoles under the following assumptions: 1) the most relevant SEY model parameters are those obtained from fits to the data obtained from Cornell Electron Storage Ring Test Accelerator (CESRTA) project's measurements for a TiN surface, 2) the distribution of photons striking the chamber surface at the location of the dipole magnet has been obtained from Synrad3d calculations, and 3) the quantum efficiency is 0.05, independent of photon energy and incident angle.

The SEY model corresponding to the above-mentioned fits yields a peak SEY value of 0.94 at an incident electron energy of 296 eV. In addition to this, we have carried out the simulation in which the SEY is set to 0 (meaning that any electron hitting the chamber walls gets absorbed with unit probability) in order to isolate the contribution to the EC density $\mathrm{N_e}$ from photoemission.

A similar simulation for the earlier DSB3 lattice [6] was made under somewhat different assumptions regarding photoemission and secondary emission. Specifically, the quantum efficiency was assumed to be 0.1, the incident photon distribution was assumed to be a simple superposition of a flat background plus a Gaussian at the photon impact point, and the SEY model was obtained from older fits to other samples and re-scaled so that the peak SEY was assumed to be 1.0. We recently repeated this simulation for DSB3 under the assumption that the quantum efficiency is 0.05, without changing any other parameters. The results for the DTC03 lattice and the new results for the DSB3 lattice are summarized in Table 1. Cloud densities averaged over the full vacuum chamber as well as those averaged over a $20\sigma_x \times 20\sigma_y$ elliptical cross-sectional area are shown. These modeling statistical uncertainties are at the level of less than 30%.

To summarize: 1) The cloud density $\mathrm{N_e}$ in an arc dipole for DTC03 is roughly twice that for DSB3, 2) This factor of about two is a direct consequence of the doubling of the photoemission rate for DTC03 relative to DSB3, 3) The factor of two is present whether the peak SEY is 0 or 0.94, 4) The results for peak SEY=0 (no secondary electrons) amount to a lower limit on $\mathrm{N_e}$, 5) However, one must keep in mind that this lower limit is directly proportional to the quantum efficiency, assumed here to be 0.05, 6) For peak SEY=0.94, $\mathrm{N_e}$ is a factor of 2 or 3 greater than that for SEY=0, both for DSB3 and DTC03, 7) These results for peak SEY=0.94 represent an upper limit for those expected for a grooved surface, 8) The 20σ $\mathrm{N_e}$ is somewhat smaller than the above-quoted overall average $\mathrm{N_e}$, 9) Ditto for the 20σ $\mathrm{N_e}$ prior to bunch passage.

EC BUILDUP IN THE QUADRUPOLES, SEXTUPOLES AND FIELD-FREE REGIONS

The EC buildup modeling code ECLOUD served to calculate estimates of the cloud densities in the quadrupoles and sextupoles in the arc and wiggler regions and in the field-free regions of the wiggler sections for the DTC03 lattice. The photon transport modeling code Synrad3d provided azimuthal photon absorption distributions average over each of these regions. The POSINST photoelectron production and SEY model parameters were also used in ECLOUD. Representative field strengths of 10 T/m (70 T/m^2)were used for the quadrupoles (sextupoles). Trapping effects were evident in the beam-pipe-averaged cloud densities, which had not yet reached equilibrium during the eight trains simulated, but since the trapping does

Table 1: POSINST modeling results for EC densities $\mathrm{N_e}$ (10^{11} $\mathrm{m^{-3}}$) in the dipole regions of the DTC03 and DSB3 lattices

	DSB3		DTC03	
	SEY=0	SEY=1.0	SEY=0	SEY=0.94
Cloud density at the end of a 34-bunch train	~ 0.2	~ 0.4	~ 0.5	~ 1.2
Peak 20-σ density during train	~ 0.1	~ 0.2	~ 0.2	~ 0.5
20-σ density prior to bunch passage	~ 0.1	~ 0.2	~ 0.2	~ 0.4

Table 2: POSINST and ECLOUD modeling results for the 20σ density estimates $\mathrm{N_e}$ (10^{11} $\mathrm{m^{-3}}$) just prior to each bunch passage in the DTC03 lattice design

	Field-free		Dipole		Quadrupole		Sextupole	
	Length (m)	N_e	Length (m)	N_e	Length (m)	N_e	Length (m)	N_e
Arc region 1	406	2.5	229	0.4	146	1.5	90	1.4
Arc region 2	365	2.5	225	0.4	143	1.7	90	1.3
Wiggler region	91	40	0		18	12	0	

not occur in the beam region, the 20σ densities prior to the passage of each bunch were stable after just a couple of trains. Table 2 shows the 20σ density estimates obtained assuming a peak SEY value of 0.94. The POSINST results for the arc dipoles are included in this table. The integrated ring lengths for the magnetic environment types are also shown.

The simulations for the field-free regions were repeated imposing a solenoidal magnetic field of 40 G, as is foreseen in the mitigation recommendations determined during the ECLOUD10 workshop [3]. Such a field was shown to reduce the cloud buildup in the beam region to negligible levels.

EC BUILDUP IN THE WIGGLERS

The EC build-up in the wiggler is simulated using the CLOUDLAND code. The ring length occupied by wigglers is 118 m. The simulation assumes a peak SEY of 1.2 for the copper surface of a wiggler chamber. The energy at the peak SEY is 250 eV. The photon flux used in the simulation is 0.198 photon/m/positron and a uniform azimuth distribution is assumed. A quantum efficiency of 0.1 and a beam size σ_x/σ_y = 80μ/5.5μ was used in the simulation. The peak wiggler field is 2.1 T. The beam chamber of the wiggler section includes an antechamber with 1 cm vertical aperture. A round chamber with diameter of 46 mm is used, which is a good approximation since most electrons accumulate near the horizontal center due to multipacting. The CLOUDLAND calculation shows that a beam with bunch population of 2×10^{10} and bunch spacing of 6 ns can excite strong multiplication near the horizontal center. The peak electron density seen by the last bunch along the bunch train is about 1.2×10^{13} $\mathrm{m^{-3}}$ The wiggler vacuum design foresees the inclusion of clearing electrodes. The curved electrode with width of 20 mm is located on the bottom of the chamber. The same SEY parameters as the chamber surface are assumed for the electrode. The actual electrode design has thermal spray tungsten and Alumina insulator. It was found that a positive electrode bias is extremely effective at suppressing multipacting. A positive voltage of a few hundred volts suffices. Interestingly, the suppression effect is not necessarily a monotonic function of the clearing voltage. The complication of the dynamics of electrons due to the clearing field, beam field and space-charge field results in this non-monotonic dependence. A weak positive voltage makes a very low electron density area with the same horizontal width as the electrode. The suppression of the cloud is effective only over the horizontal region covered by the electrode.

FUTURE WORK

The modeling work on EC buildup described above provides estimates of the cloud density in the region of the beam at the time of a bunch passage. The estimates are encouraging, placing an upper limit on the ring-averaged density of about 4×10^{10} $\mathrm{m^{-3}}$, about a factor of three lower than assumed in earlier instability simulations. The additional suppression provided by the grooved surfaces recommended for the arc dipole regions remains to be calculated for the DTC03 lattice [7, 8]. Based on these results, the simulation code CMAD [9] will be used to estimate instabilities arising due to the effect of the cloud on the beam bunches.

REFERENCES

[1] J.A. Crittenden *et al.*, TUPPR065, these proceedings

[2] J.P. Shanks *et al.*, TUPPR066, these proceedings

[3] M.T.F. Pivi *et al.*, TUPC030, proceedings of IPAC2011

[4] J.V. Conway *et al.*, TUPPR062, these proceedings

[5] G.F. Dugan and D.C. Sagan, *Proceedings of the 49th ICFA Advanced Beam Dynamics Workshop*

[6] M.A. Furman, LBNL-4474E/CBP-874

[7] L. Wang *et al.*, FRPMS079, proceedings of PAC07

[8] M. Venturini *et al.*, THPMN118, proceedings of PAC07

[9] M.T.F. Pivi *et al.*, THPAS066, proceedings of PAC07